Chapter 6

top quark decay into charged Higgs boson in a general Two-Higgs-Doublet model: Implications for the TEVATRON data

We analyze the unconventional top quark decay mode $t \to H^+ b$ at the quantum level within the context of general Two-Higgs-Doublet models by including the full electroweak effects from the Yukawa couplings. The results are presented in the on-shell renormalization scheme with a physically well motivated definition of $\tan\beta$, as explained in Sec. 4.3.2. While the QCD corrections have been taken into account in the current experimental analyses of that decay, the electroweak effects have always been neglected. However, we find that they can be rather large and could dramatically alter the interpretation of the present data from the Tevatron collider. For instance, in large portions of the parameter space the electroweak effects prevent the Tevatron data from placing any bound at all to the charged Higgs mass for essentially any value of $\tan\beta$.

6.1 Motivation

With the discovery of the top quark at the Tevatron [5, 6] the last matter building block of the Standard Model (SM) has been fully accounted for by experiment. Still, for an effective experimental underpinning of the fundamental mass generation mechanism in the SM one has to find the elementary Higgs scalar, which has intriguingly evaded all attempts up to now. Therefore, in spite of the great significance of the top quark discovery, the Higgs mechanism – the truly theoretical core of the SM – remains experimentally unconfirmed.

On the other hand, the recent evidence for the possibility of neutrino oscillations [8, 9] gives further support to the idea that the SM could be subsumed within a larger and more fundamental theory. The search for physics beyond the SM, therefore, has to continue with strong effort both at low and high energy. And, complementary to the low-energy experiments, the peculiar nature of the top quark – its large mass and its characteristic interactions with the scalar particles – may help decisively to unearth further vestiges of physics beyond the SM.

In case that the charged Higgs boson is light enough, the top quark could decay via the non-standard channel $t \to H^+ b$. Based on this possibility the CDF collaboration at the Tevatron has undertaken an experimental program which at the moment has been used to put limits on the parameter space of Type II models [56, 57].

The bounds are obtained by searching for an excess of the cross-section $\sigma(p\bar{p} \to t\bar{t}X \to \tau\nu_\tau X)$ with respect to $\sigma(p\bar{p} \to t\bar{t}X \to l\nu_l X)$ $(l = e, \mu)$. The absence of such an excess determines an upper bound on $\Gamma(t \to H^+ b \to \tau^+ \nu_\tau b)$ and a corresponding excluded region of the parameter space $(\tan\beta, M_{H^\pm})$.

However, it has been shown that the one-loop quantum corrections to that decay width can be rather large. This applies not only to the conventional QCD one-loop corrections [165, 166] – the only ones used in Ref. [56,57] – but also to the QCD and electroweak corrections in the framework of the MSSM [46, 151]. Thus the CDF limits could be substantially modified by radiative corrections [167] and in some cases the bound even disappears.

6.2 Experimental situation and Lowest order relations

To our knowledge, and in spite of some existing approximate calculations[1], a fully-fledged account of the main electroweak corrections to $\Gamma(t \to H^+ b)$ in the framework of general 2HDM's is lacking in the literature. Thus, we address the complete computation of the one-loop electroweak contributions (EW) at leading order in both λ_t and λ_b (Cf. eq. 2.5) in generic Type I and Type II 2HDM's and explore their impact on the Tevatron data. Clearly, a detailed treatment of $\Gamma(H^+ \to \tau^+ \nu_\tau)$ at the quantum level is also mandatory to perform this analysis in a consistent way.

We remark that although CLEO data on $BR(b \to s\gamma)$ could preclude the existence of a light charged Higgs boson [132] – thus barring the possibility of the top quark decaying into it – this assertion is not completely general and, moreover, needs further experimental confirmation. In fact, there is no direct experiment (at the level of the Tevatron analysis under consideration) supporting the indirect implications on charged higgses from radiative B-meson decays. Originally, the bounds from CLEO data were based on the computation up to leading order (LO) of $BR(b \to s\gamma)$ [122]. However, to this order the theoretical result suffered from very large uncertainties [170, 171]. Recently the next to leading order (NLO) calculation has become available [131, 172, 173], and the theoretical situation seems to be settling. The NLO calculation shows that Type I charged Higgs bosons masses are not restricted by $b \to s\,\gamma$ decay data either because of falling inside the experimental band or because of being not reliable. As for Type II charged Higgs bosons, a lower bound of $\sim 255\,GeV$, with an error of at most several tens of GeV, has been achieved using the conservative (95% C.L.) CLEO allowed band $BR(b \to s\gamma) = (1.0 - 4.2) \times 10^{-4}$ [132]. Nevertheless, as stated, the experimental situation is not completely settled. Recently CLEO has presented the preliminary new result $BR(b \to s\gamma) = (3.15 \pm 0.35 \pm 0.32 \pm 0.26) \times 10^{-4}$ which modifies the upper limit above to 4.5×10^{-4} [174] and, therefore, it weakens the previous bound on the charged Higgs mass. On the other hand the ALEPH result is $BR(b \to s\gamma) = (3.11 \pm 0.80 \pm 0.72) \times 10^{-4}$ [175] which implies an upper limit (90% C.L.) of 4.9×10^{-4}. Although both results are fully compatible,

[1] See [168, 169] and references therein. Because of the approximations used, neither of these references was really sensitive to the potentially large quantum effects reported here at low and high $\tan\beta$.

the latter entails a lower bound on the charged Higgs mass of $\sim 150\, GeV$ at large $\tan\beta$ [173]– thus allowing $t \to H^+ b$ also for Type II models. It is our aim to investigate, independent of and complementary to the indirect constraints, the decay $t \to H^+ b$ in general 2HDM's (Types I and II) by strictly taking into consideration the direct data from Tevatron on equal footing as in Ref. [56–58]. This study [54, 55] is complementary to the supersymmetric one in Ref. [167] and it should be useful to distinguish the kind of quantum effects expected in general 2HDM's as compared to those foreseen within the context of the MSSM.

The interaction Lagrangian describing the $H\,t\,b$-vertex in Type-j 2HDM ($j = I, II$) is:

$$\mathcal{L}^{(j)}_{Htb} = \frac{g}{\sqrt{2} M_W} H^- \bar{b}\, [m_t\, \cot\beta\, P_R + m_b\, a_j\, P_L]\, t + \text{h.c.} \tag{6.1}$$

where the parameter a_j has been defined in eq.2.6:

$$a_I \quad \equiv \quad -\cot\beta \quad a_{II} \quad \equiv \quad +\tan\beta$$

From the interaction Lagrangian (6.1) it is patent that for Type I models the branching ratios $BR(t \to H^+ b)$ and $BR(H^+ \to \tau^+ \nu_\tau)$ are relevant only at low $\tan\beta$, whereas for Type II models the former branching ratio can be important both at low and high $\tan\beta$ and the latter is only significant at high values of $\tan\beta$.

6.3 One-loop Corrected $\Gamma(t \to H^+ b)$ in the MSSM

The renormalization procedure required for the one-loop amplitude closely follows that of Sec. 4.3. For Type II models the one-loop counterterm and vertex structures are formally as in Ref. [46], whereas for Type I there are some differences. Nonetheless the two types of 2HDM's can be treated simultaneously within a unified formalism as follows: The counterterm Lagrangian $\delta\mathcal{L}^{(j)}_{Hbt}$ for each 2HDM model $j = I, II$ reads

$$\delta\mathcal{L}^{(j)}_{Hbt} = \frac{g}{\sqrt{2}\, M_W}\, H^- \bar{b} \left[\delta C^{(j)}_R\; m_t\; \cot\beta\; P_R + \delta C^{(j)}_L\; m_b\, a_j\, P_L\right] t + \text{h.c.}\,, \tag{6.2}$$

with

$$\begin{aligned}
\delta C^{(j)}_R &= \frac{\delta m_t}{m_t} - \frac{\delta v}{v} + \frac{1}{2}\,\delta Z_{H^+} + \frac{1}{2}\,\delta Z^b_L + \frac{1}{2}\,\delta Z^t_R - \frac{\delta\tan\beta}{\tan\beta} + \delta Z_{HW}\; \tan\beta\,, \\
\delta C^{(j)}_L &= \frac{\delta m_b}{m_b} - \frac{\delta v}{v} + \frac{1}{2}\,\delta Z_{H^+} + \frac{1}{2}\,\delta Z^t_L + \frac{1}{2}\,\delta Z^b_R \mp \frac{\delta\tan\beta}{\tan\beta} - \delta Z_{HW}\, \frac{1}{a_j}\,,
\end{aligned} \tag{6.3}$$

where in the last expression the upper minus sign applies to Type I models and the lower plus sign to Type II – hereafter we will adopt this convention.

The counterterm $\delta \tan\beta / \tan\beta$ is defined in such a way that it absorbs the one-loop contribution to the decay width $\Gamma(H^+ \to \tau^+ \nu_\tau)$, yielding

$$\frac{\delta \tan\beta}{\tan\beta} = \mp \left[\frac{\delta v}{v} - \frac{1}{2}\delta Z_{H^\pm} + \delta Z_{HW} \frac{1}{a_j} + \Delta_\tau^{(j)} \right] . \tag{6.4}$$

The quantity

$$\Delta_\tau^{(j)} = -\frac{\delta m_\tau}{m_\tau} - \frac{1}{2}\delta Z_L^{\nu_\tau} - \frac{1}{2}\delta Z_R^\tau - F_\tau^{(j)} , \tag{6.5}$$

contains the (finite) process-dependent part of the counterterm, where F_τ comprises the complete set of one-particle-irreducible three-point functions of the charged Higgs decay into $\tau^+ \nu_\tau$.

Substituting (6.4) into (6.3) one finally gets for the Type-j model

$$\begin{aligned} \delta C_R^{(j)} &= 2\delta_{j\,II} \left[\frac{1}{2}\,\delta Z_{H^+} - \frac{\delta v}{v} \right] + \delta Z_{HW} \left[\tan\beta \pm \frac{1}{a_j} \right] \\ &\quad + \frac{\delta m_t}{m_t} + \frac{1}{2}\,\delta Z_L^b + \frac{1}{2}\,\delta Z_R^t \pm \Delta_\tau^{(j)} \\ \delta C_L^{(j)} &= \frac{\delta m_b}{m_b} + \frac{1}{2}\,\delta Z_L^t + \frac{1}{2}\,\delta Z_R^b + \Delta_\tau^{(j)} . \end{aligned} \tag{6.6}$$

We immediately see that for Type I models the one-loop correction is free of "universal" contributions as could be expected from our definition of $\tan\beta$ (Sec. 4.3.2).

The correction to the decay width in each 2HDM can be written in the following way:

$$\begin{aligned} \delta_{\rm 2HDM}^{(j)} &= \frac{\Gamma^{(j)}(t \to H^+ b) - \Gamma_0^{(j)}(t \to H^+ b)}{\Gamma_0^{(j)}(t \to H^+ b)} \\ &= \frac{N_L^{(j)}}{D^{(j)}}[2\,\mathrm{Re}(\Lambda_L^{(j)})] + \frac{N_R}{D^{(j)}}[2\,\mathrm{Re}(\Lambda_R^{(j)})] + \frac{N_{LR}^{(j)}}{D^{(j)}}[2\,\mathrm{Re}(\Lambda_L^{(j)} + \Lambda_R^{(j)})] , \end{aligned} \tag{6.7}$$

where the lowest-order width in the on-shell α-scheme is

$$\Gamma_0^{(j)}(t \to H^+ b) = \frac{\alpha}{s_W^2} \frac{D^{(j)}}{16\, M_W^2\, m_t} \lambda^{1/2}(1, \frac{m_b^2}{m_t^2}, \frac{M_{H^\pm}^2}{m_t^2}) , \tag{6.8}$$

with

$$D^{(j)} = (m_t^2 + m_b^2 - M_{H^\pm}^2)(m_t^2\, \cot^2\beta + m_b^2\, a_j^2) + 4 m_t^2\, m_b^2\, a_j\, \cot\beta$$

$$
\begin{aligned}
N_L^{(j)} &= (m_t^2 + m_b^2 - M_{H^\pm}^2) m_b^2 \, a_j^2 \\
N_R &= (m_t^2 + m_b^2 - M_{H^\pm}^2) m_t^2 \, \cot^2\beta \\
N_{LR}^{(j)} &= 2\, m_t^2 \, m_b^2 \, a_j \, \cot\beta \, . \qquad (6.9)
\end{aligned}
$$

The corresponding correction in the G_F-scheme is [46]: $\delta(G_F) = \delta - \Delta r$.

The renormalized one-loop vertices $\Lambda_{L,R}$ for each type of model are obtained after adding up the counterterms (6.6) to the one-loop form factors:

$$
\begin{aligned}
\Lambda_L &= \delta C_L + F_L \\
\Lambda_R &= \delta C_R + F_R \, . \qquad (6.10)
\end{aligned}
$$

The one-loop Feynman diagrams contributing to the decay $t \to H^+ b$ under consideration can be seen in: Fig. 6.1, Fig. 4.14 (diagrams C_{b3}, C_{b4}), Fig. 4.15 (diagrams C_{t3}, C_{t4}), Fig. 4.16 (diagram C_{H1}, C_{H5}, C_{H6}) and Fig. 4.17 (diagram C_{M1}, C_{M4}). It goes without saying that the calculation of these diagrams in general 2HDM's is different from that in Ref. [46], and this is so even for the Type II case since some of the Higgs boson Feynman rules for supersymmetric models [67] cannot be borrowed without a careful adaptation of the couplings as made evident in Sec. 2.1.1. In the following we quote the expressions for the unrenormalized vertex functions F_L and F_R (and $F_\tau \equiv F_L^\tau$ above) for each 2HDM; the calculation and conventions follow those in Ref. [46] and make extensive use of the notation defined in Sec. 2.1.1.

6.3.1 Higgs vertex diagrams

The contributions arising from the exchange of virtual Higgs particles and Goldstone bosons in the Feynman gauge, as shown in Fig. 6.1, are:

- Diagram (V_{H1}):

$$
\begin{aligned}
F_L &= N\,[m_b^2 (C_{12} - C_0) + m_t^2 \frac{\cot\beta}{a_j} (C_{11} - C_{12})] \, , \\
F_R &= N m_b^2 [C_{12} - C_0 + \frac{a_j}{\cot\beta} (C_{11} - C_{12})] \, , \\
N &= -\frac{ig^2}{2} \{R_j, r_j\} N_1 \, ,
\end{aligned}
$$

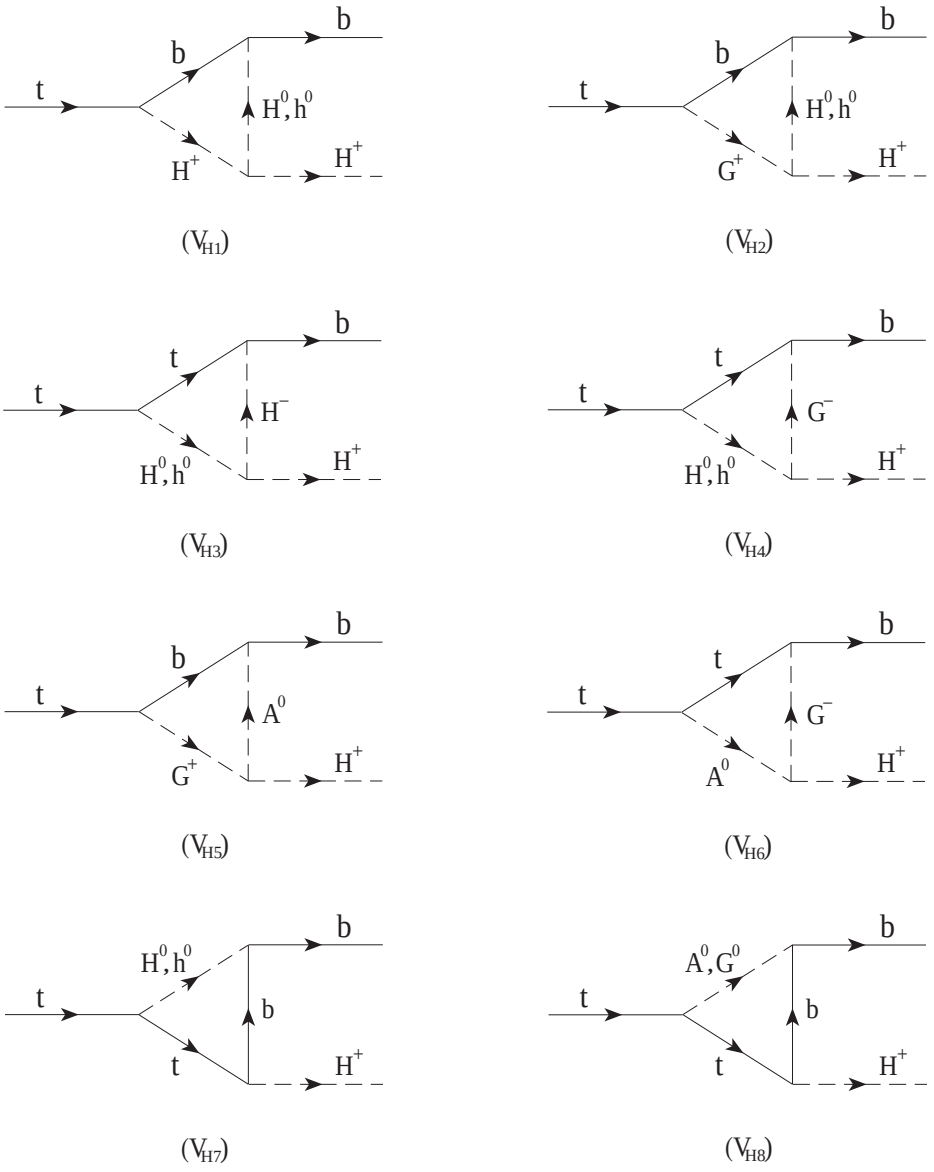

Figure 6.1: *Feynman diagrams, up to one-loop order, for the Higgs and Goldstone boson vertex corrections to the decay process* $t \to H^+ b$.

$$
\begin{aligned}
N_1 &= \frac{M^2_{A^0} - m^2_{\{H_0,h_0\}}}{M^2_W} \cot 2\beta \{\sin(\alpha-\beta), \cos(\alpha-\beta)\} + \\
&\quad \frac{M^2_{A^0} - M^2_{H^\pm} - m^2_{\{H_0,h_0\}}/2}{M^2_W} \{\cos(\beta-\alpha), \sin(\beta-\alpha)\}\,, \\
C_* &= C_*\left(p, p', m_b, M_{H^\pm}, \{M_{H^0}, M_{h^0}\}\right)\,.
\end{aligned}
$$

- Diagram (V_{H2}):

$$
\begin{aligned}
F_L &= N \frac{1}{a_j} [m_t^2 (C_{11} - C_{12}) + m_b^2 (C_0 - C_{12})]\,, \\
F_R &= N m_b^2 \tan\beta (2C_{12} - C_{11} - C_0)\,, \\
N &= \pm \frac{ig^2}{4} \{R_j, r_j\} \{\sin(\beta-\alpha), \cos(\beta-\alpha)\} \left(\frac{M^2_{H^\pm}}{M^2_W} - \frac{\{M^2_{H^0}, M^2_{h^0}\}}{M^2_W} \right)\,, \\
C_* &= C_*\left(p, p', m_b, M_W, \{M_{H^0}, M_{h^0}\}\right)\,.
\end{aligned}
$$

- Diagram (V_{H3}):

$$
\begin{aligned}
F_L &= N m_t^2 [\frac{\cot\beta}{a_j} C_{12} + C_{11} - C_{12} - C_0]\,, \\
F_R &= N [m_b^2 \frac{a_j}{\cot\beta} C_{12} + m_t^2 (C_{11} - C_{12} - C_0)]\,, \\
N &= -\frac{ig^2}{2} \frac{\{\sin\alpha, \cos\alpha\}}{\sin\beta} N_1\,, \\
C_* &= C_*\left(p, p', m_t, \{M_{H^0}, M_{h^0}\}, M_{H^\pm}\right)\,.
\end{aligned}
$$

- Diagram (V_{H4}):

$$
\begin{aligned}
F_L &= N m_t^2 (2C_{12} - C_{11} + C_0) \frac{1}{a_j}\,, \\
F_R &= N [-m_b^2 C_{12} + m_t^2 (C_{11} - C_{12} - C_0)] \tan\beta\,, \\
N &= \mp \frac{ig^2}{4} \frac{\{\sin\alpha, \cos\alpha\}}{\sin\beta} \{\sin(\beta-\alpha), \cos(\beta-\alpha)\} \left(\frac{M^2_{H^\pm}}{M^2_W} - \frac{\{M^2_{H^0}, M^2_{h^0}\}}{M^2_W} \right)\,, \\
C_* &= C_*\left(p, p', m_t, \{M_{H^0}, M_{h^0}\}, M_W\right)\,.
\end{aligned}
$$

- Diagram (V_{H5}):

$$
F_L = N [m_b^2 (C_{12} + C_0) + m_t^2 (C_{11} - C_{12})]\,,
$$

$$
\begin{aligned}
F_R &= N m_b^2 \frac{a_j}{\cot\beta}(C_{11} + C_0)\,, \\
N &= -\frac{ig^2}{4}\left(\frac{M_{H^\pm}^2}{M_W^2} - \frac{M_{A^0}^2}{M_W^2}\right)\,, \\
C_* &= C_*\,(p, p', m_b, M_W, M_{A^0})\ .
\end{aligned}
$$

- Diagram (V_{H6}):

$$
\begin{aligned}
F_L &= N m_t^2 \frac{\cot\beta}{a_j}(C_{11} + C_0)\,, \\
F_R &= N\,[m_b^2 C_{12} + m_t^2(C_{11} - C_{12} + C_0)]\,, \\
N &= -\frac{ig^2}{4}\left(\frac{M_{H^\pm}^2}{M_W^2} - \frac{M_{A^0}^2}{M_W^2}\right)\,, \\
C_* &= C_*\,(p, p', m_t, M_{A^0}, M_W)\ .
\end{aligned}
$$

- Diagram (V_{H7}):

$$
\begin{aligned}
F_L &= N[(2m_b^2 C_{11} + \tilde{C}_0 + 2(m_t^2 - m_b^2)(C_{11} - C_{12}))\frac{\cot\beta}{a_j} + 2m_b^2(C_{11} + 2C_0)]m_t^2, \\
F_R &= N[(2m_b^2 C_{11} + \tilde{C}_0 + 2(m_t^2 - m_b^2)(C_{11} - C_{12}))\frac{a_j}{\cot\beta} + 2m_t^2(C_{11} + 2C_0)]m_b^2, \\
N &= \frac{ig^2}{4M_W^2}\left\{\frac{\sin\alpha}{\sin\beta}R_j\,, \frac{\cos\alpha}{\sin\beta}r_j\right\}\,, \\
C_* &= C_*\,(p, p', \{M_{H^0}, M_{h^0}\}, m_t, m_b)\ .
\end{aligned}
$$

- Diagram (V_{H8}):

$$
\begin{aligned}
F_L &= N m_t^2 \{\frac{\cot\beta}{a_j}\,, \cot^2\beta\}\,\tilde{C}_0\,, \\
F_R &= N m_b^2 \{\frac{a_j}{\cot\beta}\,, \tan^2\beta\}\,\tilde{C}_0\,, \\
N &= \mp\frac{ig^2}{4M_W^2}\,, \\
C_* &= C_*\,(p, p', \{M_{A^0}, M_Z\}, m_t, m_b)\ .
\end{aligned}
$$

6.3.2 Counterterms

- Counterterms $\delta m_f\,, \delta Z_L^f\,, \delta Z_R^f$: For a given down-like fermion b, and corresponding isospin partner t, the fermionic self-energies receive, in the Feynman gauge, the following contributions from Higgs and Goldstone bosons.

$$
\begin{aligned}
\Sigma^b_{\{L,R\}}(p^2) &= \Sigma^b_{\{L,R\}}(p^2)\Big|_{(C_{b3})+(C_{b4})} \\
&= \frac{g^2}{2iM_W^2}\left\{m^2_{\{t,b\}}\left[\{\cot^2\beta, a_j^2\}B_1(p,m_t,M_{H^\pm}) + B_1(p,m_t,M_W)\right]\right. \\
&+ \frac{m_b^2}{2}\Big[R_j^2\, B_1(p,m_b,M_{H^0}) + r_j^2\, B_1(p,m_b,M_{h^0}) \\
&\quad \left. + a_j^2\, B_1(p,m_b,M_{A^0}) + B_1(p,m_b,M_Z)\Big]\right\}\,, \\
\Sigma^b_S(p^2) &= \Sigma^b_S(p^2)\Big|_{(C_{b3})+(C_{b4})} \\
&= -\frac{g^2}{2iM_W^2}\left\{m_t^2 a_j\cot\beta\,[B_0(p,m_t,M_{H^\pm}) - B_0(p,m_t,M_W)]\right. \\
&+ \frac{m_b^2}{2}\Big[R_j^2\, B_0(p,m_b,M_{H^0}) + r_j^2\, B_0(p,m_b,M_{h^0}) \\
&\quad \left. - a_j^2\, B_0(p,m_b,M_{A^0}) - B_0(p,m_b,M_Z)\Big]\right\}\,,
\end{aligned}
\tag{6.11}
$$

To obtain the corresponding expressions for an up-like fermion, t, just perform the label substitutions $b \leftrightarrow t$ on eqs. (4.60)-(6.11); and on eq. (6.11) substitute $R_j \to \sin\alpha/\sin\beta$, $r_j \to \cos\alpha/\sin\beta$ and replace $a_j \leftrightarrow \cot\beta$).

Introducing the above expressions into eqs. (3.27)-(3.27) one immediately obtains the SUSY contribution to the counterterms $\delta m_f\,, \delta Z^f_{L,R}$.

- Counterterm $\delta Z_{H^\pm}$:

$$
\begin{aligned}
\delta Z_{H^\pm} &= \delta Z_{H^\pm}|_{(C_{H1})+(C_{H5})+(C_{H6})} = \Sigma'_{H^\pm}(M^2_{H^\pm}) \\
&= -\frac{ig^2 N_C}{M_W^2}\Big[(m_b^2 a_j^2 + m_t^2\cot^2\beta)(B_1 + M^2_{H^\pm}B_1' + m_b^2 B_0') \\
&\qquad + 2\cot\beta a_j m_b^2 m_t^2 B_0'\Big]\,(M_{H^\pm}, m_b, m_t) \\
&\quad + ig^2\sum_{AB}\left|M^{H^+}_{AB}\right|^2 B_0'(M_{H^\pm}, m_{H_A}, m_{H_B})\,.
\end{aligned}
\tag{6.12}
$$

where m_{H_A} is either the charged Higgs mass or the charged Goldstone mass (m_{W^+} and m_{H_B} is one of neutral Higgses or the Neutral Goldstone mass (m_Z) (Cf. eq. 2.8). Notice that diagrams (C_{H3}) and (C_{H5}) give a vanishing contribution to $\delta Z_{H^\pm}$.

- Counterterm δZ_{HW}:

$$\begin{aligned}\delta Z_{HW} &= \delta Z_{HW}|_{(C_{M1})} = \frac{\Sigma_{HW}(M^2_{H^\pm})}{M^2_W} \\ &= -\frac{ig^2 N_C}{M^2_W}\left[m_b^2 a_j(B_0+B_1) + m_t^2 \cot\beta B_1\right](M_{H^\pm}, m_b, m_t) \\ &\quad -ig^2 \sum_{AB} M^{H^+}_{AB} M^{W^+}_{AB} \left[2B_1 + B_0\right](M_{H^\pm}, m_{H_A}, m_{H_B})\,. \end{aligned} \tag{6.13}$$

where a sum is understood over all generations, and $M^{W^+}_{AB}$ is given in eq. 4.66.

6.3.3 Analytical leading contributions

From the above formulæ, it is straightforward to derive the leading terms in the large Higgs boson splitting and $\cot\beta$ regime and thus foreseing in an easy way the behaviour with the different parameters.

For the Type I model the leading contributions come from the F_R form-factor and originate in diagrams C_{H3}, C_{H4}, C_{H6}. explicitly the leading parts are:

- Diagram (V_{H3}):

$$\begin{aligned} F_R &\approx \frac{ig^2 m_t^2}{2M^2_W \sin\beta}\left(\frac{1}{2}\cot\beta\{\sin^2\alpha\,,\cos^2\alpha\}(M^2_{A^0} - \{M^2_{H^0}\,, M^2_{h^0}\}) \right. \\ &\qquad \left. \mp \sin\alpha\cos\alpha(M^2_{A^0} - M^2_{H^\pm} - \frac{1}{2}\{M^2_{H^0}\,, M^2_{h^0}\})\right) \\ &\qquad \times \left[(C_{11} - C_{12} - C_0)\right](p, p', m_t, \{M_{H^0}, M_{h^0}\}, M_{H^\pm}) \end{aligned} \tag{6.14}$$

- Diagram (V_{H4}):

$$\begin{aligned} F_R &\approx \pm\frac{ig^2 m_t^2}{4M^2_W \sin\beta}\{\sin^2\alpha\,,\cos^2\alpha\}(M^2_{H^\pm} - \{M^2_{H^0}\,, M^2_{h^0}\}) \\ &\qquad \times \left[(C_{11} - C_{12} - C_0)\right](p, p', m_t, \{M_{H^0}, M_{h^0}\}, M_W) \end{aligned} \tag{6.15}$$

- Diagram (V_{H6}):

$$\begin{aligned} F_R &\approx -\frac{ig^2 m_t^2}{4M^2_W}\{\sin^2\alpha\,,\cos^2\alpha\}(M^2_{H^\pm} - M^2_{A^0}) \\ &\qquad \times \left[(C_{11} - C_{12} - C_0)\right](p, p', m_t, M_{A^0}, M_W) \end{aligned} \tag{6.16}$$

Thus, quantum effects will be sensitive to the splitting of Higgs boson masses, to $\cot\beta$ and to $\sin^2\alpha + \cos^2\alpha$ –which becomes more clear adding up the CP even neutral boson Higgs contributions. Nevertheless, (V_{H6}) does not depend on β or α, so a constant part will appear.

For the Type II model the leading contribution arise in the F_L form-factor and come from diagrams (V_{H3}) . The leading terms are:

- Diagram (V_{H3}):

$$\begin{aligned} F_L &\approx \pm\frac{ig^2 m_t^2 \tan\beta}{4M_W^2}\sin(2\alpha)(M_{A^0}^2 - \{M_{H^0}^2\,, M_{h^0}^2\}) \\ &\quad \times [C_{11} - C_{12} - C_0]\,(p, p', m_t, \{M_{H^0}, M_{h^0}\}, M_{H^\pm}) \end{aligned} \tag{6.17}$$

- Diagram (V_{H5}):

$$F_L \approx \frac{ig^2 m_t^2}{4M_W^2}(M_{H^\pm}^2 - M_{A^0}^2)[(C_{12} - C_{11})]\,(p, p', m_b, M_W, M_{A^0}) \tag{6.18}$$

- Diagram (V_{H7}):

$$\begin{aligned} F_L &\approx \pm\frac{ig^2 \sin(2\alpha) m_t^2}{4\sin(2\beta)M_W^2} \\ &\quad \times [(2m_b^2 C_{11} + \tilde{C}_0 + 2(m_t^2 - m_b^2)(C_{11} - C_{12}))\cot^2\beta \\ &\quad + 2m_b^2(C_{11} + 2C_0)]\,(p, p', \{M_{H^0}, M_{h^0}\}, m_t, m_b) \end{aligned} \tag{6.19}$$

6.4 Numerical analysis of the quantum corrections to $t \to H^+ b$

In the numerical analysis presented in Figs. 6.2-6.5 we have put several cuts on our set of inputs. From the study of the Bjorken process $e^+ e^- \to Z h^0$ and the Higgs boson pair production $e^+ e^- \to h^0 A^0$ one obtains [2]

$$M_{h^0} + M_{A^0} \gtrsim 90 - 110\, GeV\,, \tag{6.20}$$

[2] See Ref. [176] for a review and references therein.

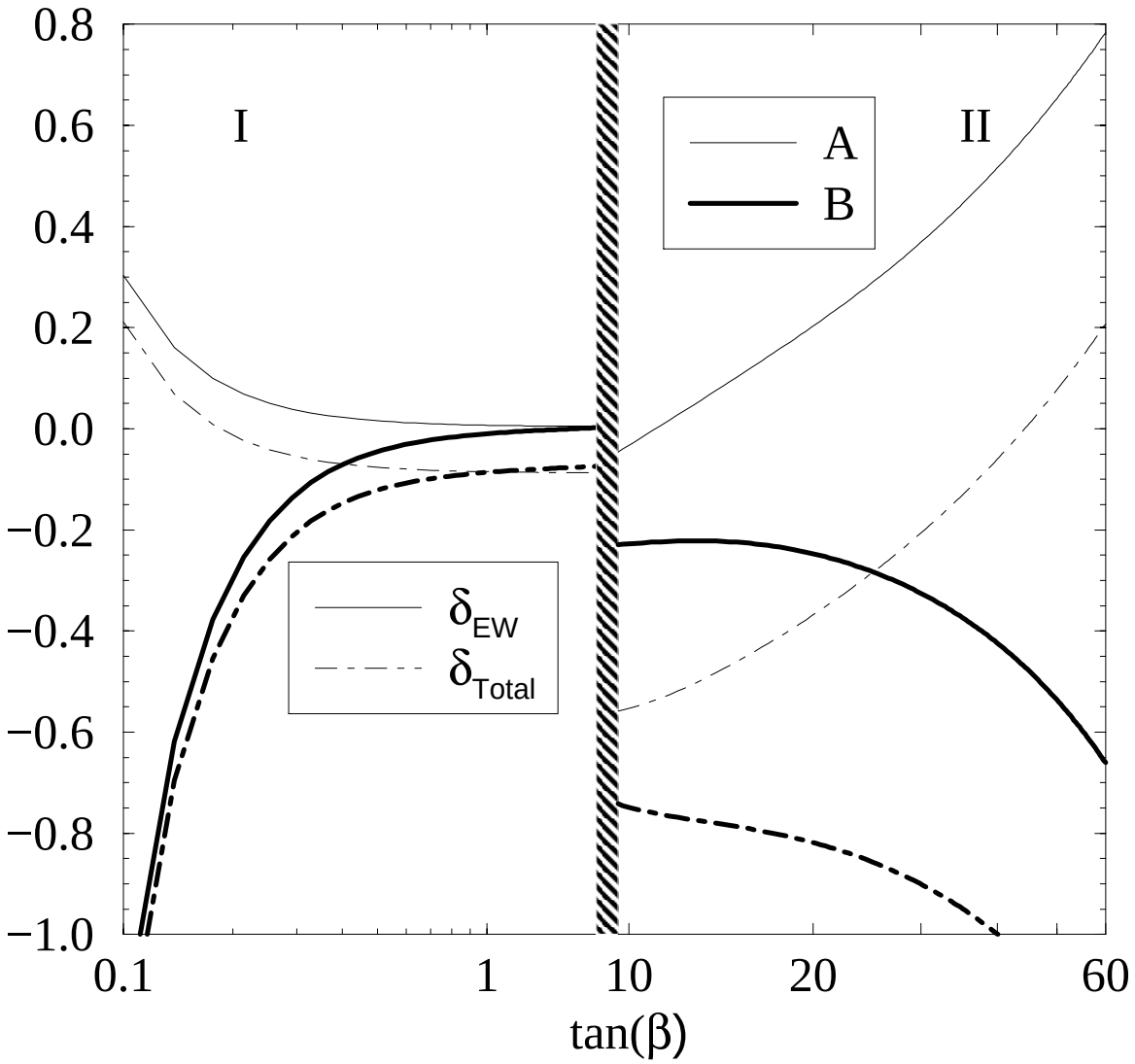

Figure 6.2: *The correction δ, eq. (6.7), to the decay width $\Gamma(t \to H^+ b)$ as a function of $\tan\beta$, for Type I 2HDM's (left hand side of the figure) and two sets of inputs $\{(M_{H^\pm}, M_{H^0}, M_{h^0}, M_{A^0}); \tan\alpha\}$, namely set A: $\{(70, 175, 100, 50)\, GeV;\, 3\}$ and set B: $\{(120, 200, 80, 250)\, GeV; 1\}$. Similarly for Type II models (right hand side of the figure) and for two different sets of inputs, set A: $\{(120, 300, 50, 225)\, GeV;\, 1\}$ and set B: $\{(120, 300, 80, 225)\, GeV;\, -3\}$. Shown are the electroweak contribution $\delta_{\rm EW}$ and the total correction $\delta_{\rm Total} = \delta_{\rm EW} + \delta_{\rm QCD}$.*

and hence it cannot yet be excluded the possibility of a light neutral Higgs scalar, say below $50\,GeV$, in general 2HDM's. As for $\tan\beta$ we have restricted in principle to the segment

$$0.1 \lesssim \tan\beta \lesssim 60 \ . \tag{6.21}$$

For Type I models the limits are very weak while for Type II the limit at the low $\tan\beta$ end is obtained from measurements of the process $e^+\,e^- \to Z \to h^0/A^0\,\gamma$ for $\tau^+\,\tau^-$, light quarks and b-quark decay channels [176]. We adopt the same low $\tan\beta$ limit for Type I models since in this region the analysis should be similar. For the three Higgs bosons coupling we have imposed that they do not exceed the maximum unitarity level permitted for the SM three Higgs boson coupling, i.e. [3]

$$|\lambda_{HHH}| \lesssim |\lambda^{SM}_{HHH}(m_H = 1\,TeV)| = g\frac{3}{2}\frac{(1\,TeV)^2}{M_W} \ . \tag{6.22}$$

This condition restricts both the ranges of masses and of $\tan\beta$. Moreover, we have imposed that the extra induced contributions to the ρ parameter are bounded by the current experimental limit [4] :

$$|\Delta\rho| \leq 0.003 \ . \tag{6.23}$$

With these restrictions, which are independent and truly effective in our calculation, we limit our numerical analysis within a wide region of parameter space where the correction (6.7) itself remains perturbative, except in those places where for demonstrational purposes we explicitly exhibit a departure from this requirement.

Before exploring the implications for the Tevatron analyses, we wish to show the great sensitivity (through quantum effects) of the decay $t \to H^+\,b$ to the particular structure of the underlying 2HDM. Therefore, in the following we summarize our systematic scanning over the parameter space of 2HDM's; in some cases, just to illustrate maximum effects, we have stretched their ranges to the very limits defined by conditions (6.20)-(6.23). In all cases we present our results in a significant region of the parameter space where the branching ratios

[3] A misprint in eq.(16) of Ref. [54] has been corrected

[4] Notice that this condition restrains Δr within the experimental range and *a fortiori* the corresponding corrections in the G_F-scheme. The bulk of the EW effects are contained in the non-universal corrections predicted in the α-scheme.

$BR(t \to H^+ b)$ and $BR(H^+ \to \tau^+ \nu_\tau)$ are expected to be sizable. This entails relatively light charged Higgs bosons ($M_{H^\pm} \lesssim 150\, GeV$) and a low (high) value of $\tan\beta$ for Type I (II) models.

In Fig. 6.2 we display the evolution of the correction (6.7) with $\tan\beta$ for Types I and II 2HDM's and for two sets of inputs A and B for each model. We separately show the (leading) EW contribution, $\delta_{\rm EW}$, and the total correction, $\delta_{\rm Total} \equiv \delta_{\rm EW} + \delta_{\rm QCD}$, which incorporates the conventional QCD effects [165,166]. In this figure we have skipped the interval $2 \lesssim \tan\beta \lesssim 10$ where the branching ratio of $t \to H^+ b$ is too small to be of phenomenological interest. In the relevant $\tan\beta$ segments, that is below and above the uninteresting one, we find that the pure EW contributions can be rather large, to wit: For Type I models, the positive effects can reach $\simeq 30\%$, while the negative contributions may increase 'arbitrarily' – thus effectively enhancing to a great extent the modest QCD corrections– still in a region of parameter space respecting the restrictions (6.20)-(6.23); For Type II models, instead, the EW effects can be very large, for both signs, in the high $\tan\beta$ regime. In particular, the huge positive yields could go into a complete "screening" of the QCD corrections.

In Fig. 6.3 (resp. 6.4) we present the evolution of the corrections in Type I (resp. II) models as a function of the other parameters, namely the tangent of the CP-even mixing angle (a), the charged Higgs mass (b), the CP-odd scalar mass (c) and the CP-even scalar masses (d). Inputs A and B for each model are as in Fig. 1 whenever they are fixed. Notice the rapid oscillation, yet qualitatively different for both models, around $\tan\alpha = 0$. This behaviour is the predicted in Sec. 6.3.3, were we just used the leading contributions. In the same way, the fast evolution that can be seen as a function of the masses is due to the fact that the Higgs self-couplings in the three-point functions are proportional to the splitting of the Higgs masses. In Fig. 6.3d (also in Fig. 6.4d) the range of the CP-even masses is plotted until the condition $M_{h^0} < M_{H^0}$ is exhausted or there is a breakdown of relations (6.22) and/or (6.23).

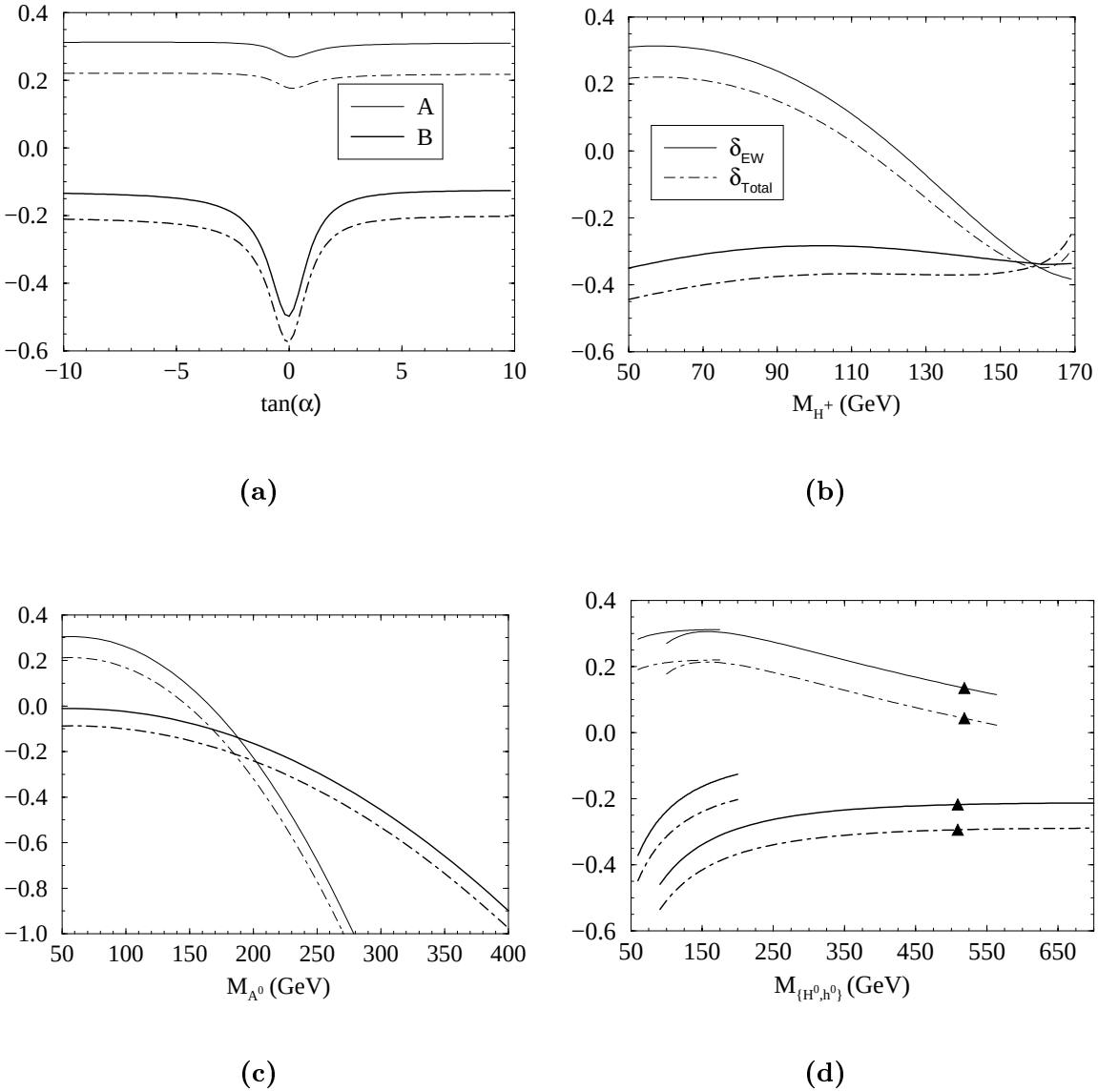

Figure 6.3: *The corrections* $\delta_{\rm EW}$ *and* $\delta_{\rm Total}$ *for the Type I 2HDM as a function of* **(a)** $\tan\alpha$, **(b)** *the charged Higgs mass,* **(c)** *the pseudoscalar Higgs mass, and* **(d)** *the heavy (labelled with a triangle) and light (unlabelled) scalar Higgs masses. Inputs as in Fig. 6.2 with* $\tan\beta = 0.1$ *for set A and* $\tan\beta = 0.2$ *for set B.*

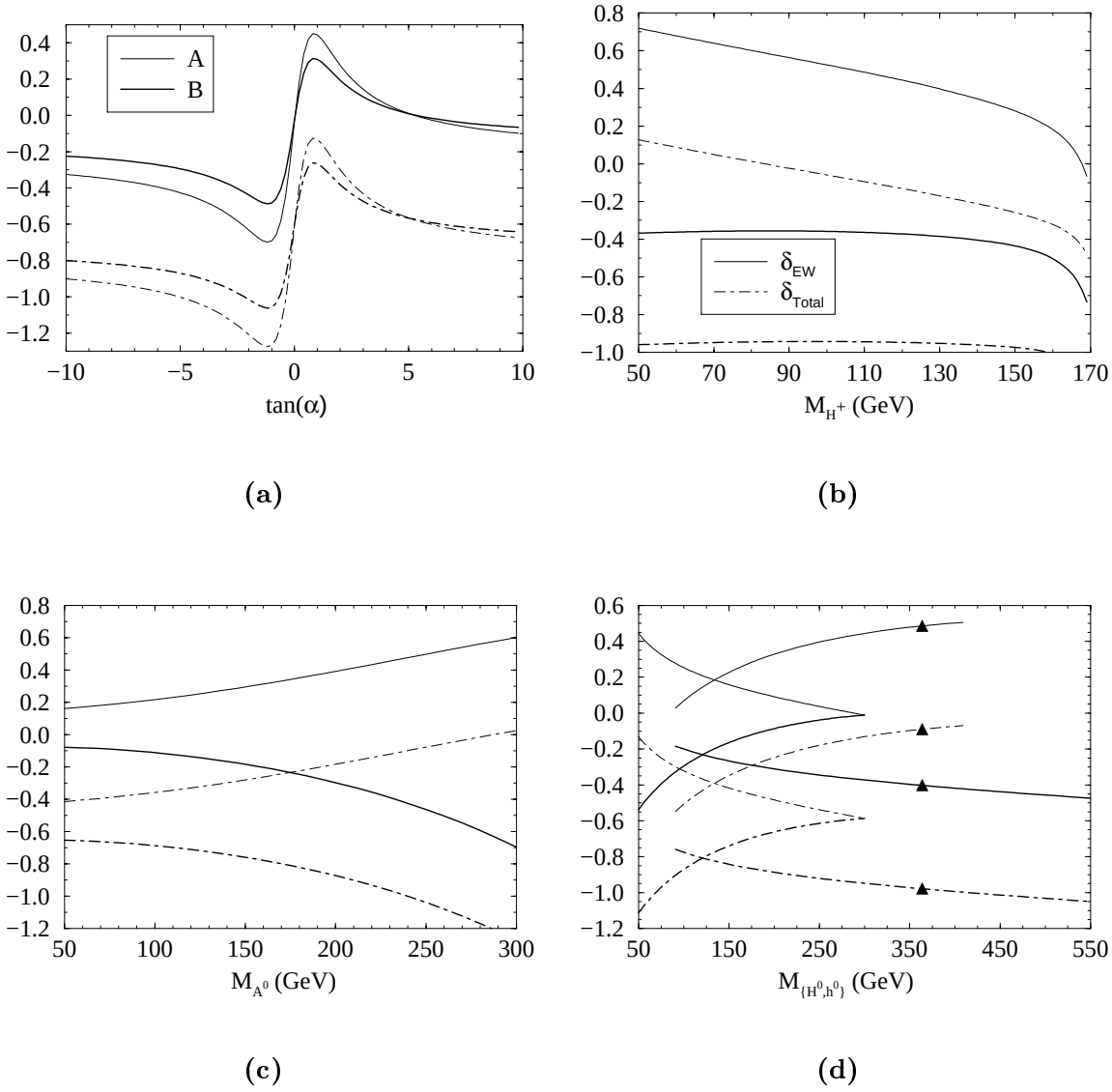

Figure 6.4: *The corrections* $\delta_{\rm EW}$ *and* $\delta_{\rm Total}$ *for the Type II 2HDM as a function of* **(a)** $\tan\alpha$, **(b)** *the charged Higgs mass,* **(c)** *the pseudoscalar Higgs mass, and* **(d)** *the heavy (labelled with a triangle) and light (unlabelled) scalar Higgs masses. Inputs as in Fig. 6.2 with* $\tan\beta = 35$ *for both sets.*

Eff. Process	$p_T^{\ell,\tau}$ & geom.	$\epsilon^{\ell}_{tr}, \epsilon^{\ell}_{iso}$, ϵ^{ℓ}_{id}, ϵ^{τ}_{id}	jets, H_T & $\not\!\!E_T$
WW	.16 (.13)	.93 × .9	.64 (.54)
$WH(80)$	.19	× .87 × .5	.61
$WH(100)$	.21	= .36	.62
$WH(120)$	.22		.64
$WH(140)$	.22		.65

Table 6.1: *The efficiency factors for the $l\tau$ channel in WW and WH decay of $t\bar{t}$ at the CDF [177]. For the WW process, the corresponding efficiencies from the CDF simulation are shown in parenthesis. The middle column shows the triggering, isolation and identification efficiencies from the CDF simulation. The total efficiencies $\epsilon_{\{1,2\}}$ are obtained by multiplying the three columns.*

6.5 The Limits on 2HDM

Next we turn to the discussion of the dramatic implications that the EW effects may have for the decay $t \to H^+ b$ at the Tevatron. The original analysis of the data (based on the non-observation of any excess of τ-events) and its interpretation in terms of limits on the 2HDM parameter space was performed in Ref. [56, 57] (for Type II models) without including the EW corrections. In these references an exclusion plot is presented in the $(\tan\beta, M_{H^\pm})$-plane after correcting for QCD effects only. To demonstrate the potential impact of the EW loops on these studies we follow the method of Ref. [167]. Although the data used by the Tevatron collaborations is based on inclusive τ-lepton tagging [56, 57], it will suffice for illustrative purposes to concentrate ourselves on the (τ,l)-channel [167, 177]. In this way the comparison of the results for generic Type II 2HDM's and those already available for the specific case of the MSSM Higgs sector [167] will be more transparent. The production cross-section of the top quark in the (τ,l)-channel can be easily related to the decay rate of $t \to H^+ b$ and the

branching ratio of $H^+ \to \tau^+ \nu_\tau$ as follows:

$$\sigma_{l\tau} = \left[\frac{4}{81}\,\epsilon_1 + \frac{4}{9}\,\frac{\Gamma(t \to H^+ b)}{\Gamma(t \to W^+ b)}\, BR(H^+ \to \tau^+ \nu_\tau)\,\epsilon_2 \right] \sigma_{t\bar{t}}\,, \tag{6.24}$$

where the first term in eq. 6.24 comes from the SM decay, and the second is the generalization of the corresponding term in eq.(7) of Ref. [167] for the case that $BR(H \to \tau\,\nu_\tau)$ is not 100%, as it indeed happens when we explore the low $\tan\beta$ region. In general we have

$$BR(H^+ \to \tau^+ \nu_\tau) = \frac{\Gamma(H^+ \to \tau^+ \nu_\tau)}{\Gamma(H^+ \to \tau^+ \nu_\tau) + \Gamma(H^+ \to c\,\bar{s})}\,, \tag{6.25}$$

where we use the QCD-corrected amplitude for the last term in the denominator [116, 117]. This branching ratio is about 50% for Type I 2HDM at low $\tan\beta$, and 100% for Type II at high $\tan\beta$ (the case studied in [167]). Finally, ϵ_i are the detector efficiency factors [177], which we quote in table 6.1. Notice that the use of the measured value of $\sigma_{t\bar{t}}$ [178], instead of the predicted value within the standard NLO QCD approach [179, 180], allows a model-independent treatment of the result. In this respect, we note that there could be MSSM effects on the standard mechanisms for $t\bar{t}$ production [181] (viz. Drell-Yan $q\bar{q}$ annihilation and gluon-gluon fusion) as well as corrections in the subsequent top quark decays [109, 110]. To be concrete, we use the following value for the top pair production cross-section [178]:

$$\sigma_{t\bar{t}} = 7.5 \pm 1.5\,\text{pb}$$

The number of events found in the (l, τ)-channel up to an integrated luminosity of 100 fb^{-1} is 4 [52, 182], with an expected background of around 2 events and 1 event expected in the SM. This implies an upper limit of 7.7 events at 95% C.L., that is

$$\sigma_{l\tau} < 70\,\text{fb}\ (95\%\ \text{C.L.})$$

Finally in Fig. 6.5 we have plotted the perturbative exclusion regions in the parameter space $(\tan\beta, M_{H^\pm})$ for intermediate and extreme sets of 2HDM inputs A, B, B' and C.

In Type I models (a) we see that the bounds obtained from the EW-corrected amplitude are generally less restrictive than those obtained by means of tree-level and QCD-corrected amplitudes. Evolution of the excluded region from set A to set C in Fig. 6.5a shows that the region tends to evanesce, which is indeed the case when we further increase M_{A^0} in set C.

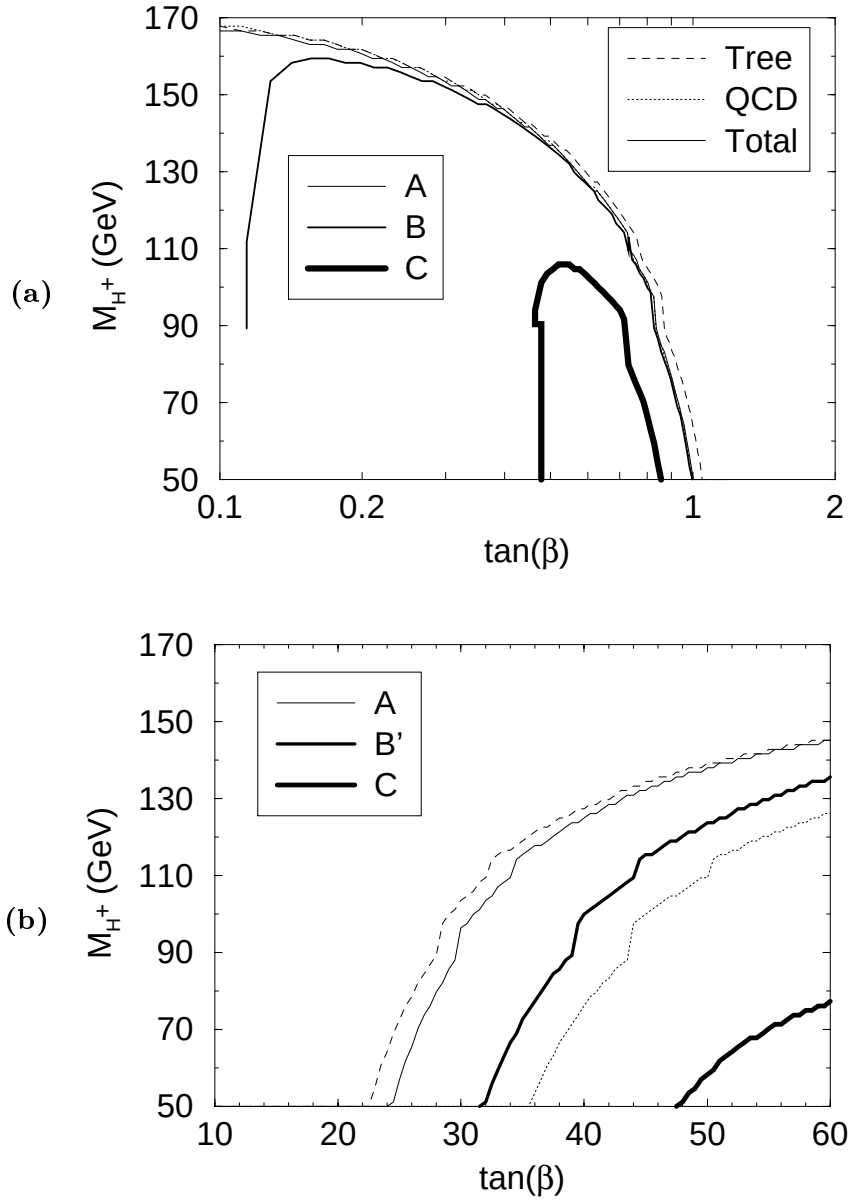

Figure 6.5: *The* 95% *C.L. exclusion plot in the* $(\tan\beta, M_{H^\pm})$*-plane for* **(a)** *Type I 2HDM using three sets of inputs: A and B as in Fig. 6.2, and C:* $\{(M_{H^\pm}, 200, 80, 700)\, GeV;\, 1\}$*;* **(b)** *Similarly for Type II models including three sets of inputs: A as defined in Fig. 6.2, B':*$\{(M_{H^\pm}, 200, 80, 150)\, GeV;\, 0.3\}$*, and C:*$\{(M_{H^\pm}, 200, 80, 150)\, GeV;\, -3\}$*. Shown are the tree-level, QCD-corrected and fully 2HDM-corrected contour lines. The excluded region in each case is the one lying below these curves.*

In Type II models (b) we also show a series of possible scenarios. We have checked that the maximum positive effect $\delta_{EW} > 0$ (set A in Fig. 6.5b) may completely cancel the QCD corrections and restore the full one-loop width $\Gamma^{(II)}(t \to H^+ b)$ to the tree-level value (6.8) just as if there were no QCD corrections at all! Intermediate possibilities (set B') are also shown. In the other extreme the (negative) effects $\delta_{EW} < 0$ enforce the exclusion region to draw back to curve C where it starts to gradually disappear into a non-perturbative corner of the parameter space where one cannot claim any bound whatsoever!!.

Some discussion may be necessary to compare the present analysis with the supersymmetric one in Refs. [46, 48, 167]. In the MSSM case, the Higgs sector is of Type II. However, due to supersymmetric restrictions in the structure of the Higgs potential, there are large cancellations between the one-particle-irreducible vertex functions, so that the overall contribution from the MSSM Higgs sector to the correction (6.7) is negligible. In fact, we have checked that when we take the Higgs boson masses as they are correlated by the MSSM we recover the previous result [46]. Still, in the SUSY case there emerges a large effect from the genuine sparticle sector, mainly from the SUSY-QCD contributions to the bottom mass renormalization counterterm [46], which can be positive or negative because the correction flips sign with the higgsino mixing parameter. In contrast, for general (non-SUSY) Type II models the bulk of the EW correction comes from large unbalanced contributions from the vertex functions, which can also flip sign with $\tan\alpha$ (Cf. Fig. 6.3a) – a free parameter in the non-supersymmetric case.

Although the size and sign of the effects can be similar for a general Type II and a SUSY 2HDM, they should be distinguishable since the large corrections are attained for very different values of the Higgs boson masses. For instance, in generic 2HDM's (of both types) large negative effects may occur for large values of the CP-odd Higgs mass (Cf. Figs. 6.3c and 6.3c). In the MSSM the latter should be essentially degenerate with the charged Higgs in that region and so $t \to H^+ b$ would have never occurred.

Therefore, just to illustrate one possibility, let us envision the following scenario. Suppose that $t \to H^+ b$ is not observed at the Tevatron – or that it comes out highly suppressed beyond QCD expectations (Cf. Fig. 6.5b, curve C) – while at the same time H^+ and A^0

are observed (maybe produced at the Tevatron itself or at LEP) and both show up with a similar mass below m_t. Then these bosons could well be supersymmetric Higgs bosons. If, however, a similar situation would be encountered but A^0 is not produced (because it is perhaps too heavy), then the observed H^+ cannot probably be a SUSY Higgs. Notice (Cf. Fig. 6.5a) that in this case the H^+ could also belong to a Type I model. In this case further investigation would be required to disentangle the type of non-SUSY Higgs model at hand e.g. aiming at a determination of $\tan\beta$. One possibility would be from the decay $H^+ \to \tau^+ \nu_\tau$ after H^+ been produced from mechanisms other than top quark decay; alternatively, once a heavy A^0 would be found it would provide a handle to a $\tan\beta$ measurement through the decays $A^0 \to \tau^+ \tau^-$ and/or $A^0 \to b\bar{b}$. If these decays would be tagged at a high rate, the non-SUSY model should necessarily be of Type II. At the LHC, or at a NLC, one could even use $\Gamma(A^0 \to b\bar{b})/\Gamma(A^0 \to t\bar{t}) \propto \tan^4\beta$ for very heavy A^0. In short, a combined procedure based on quantum effects and direct production could be a suitable strategy to unravel the identity of the Higgs bosons.

6.6 Conclusions

To summarize, we have computed the electroweak one-loop corrections to the unconventional top quark decay width $\Gamma(t \to H^+ b)$ at the leading order in the Yukawa couplings both for general Type I and Type II 2HDM's. We have found that the EW corrections can be comparable in size to the QCD effects and be of both signs. The positive ones can reach 30% and 50% for Type I and Type II models respectively, which means that they could simply delete the QCD corrections. The negative ones can even be larger (-50% or more in ample regions of parameter space) for both models. We have also shown that this fact may deeply influence the current interpretation of the Tevatron data on that decay. Most important, we have argued that knowledge of the EW quantum effects may be crucial to understand the nature (2HDM, supersymmetric...) of the Higgs bosons, if they are eventually found in future experiments at hadron and/or $e^+ e^-$ colliders.